THE AMERICAN SOCIETY OF MECHANICAL ENGINEERS
345 E. 47 St., New York, N.Y. 10017

89-GT-159

Verification of an Impeller Design by Laser Measurements and 3D-Viscous Flow Calculations

H. KRAIN
W. HOFFMAN
DFVLR, Institut für Antriebstechnik
Linder Höhe, 5000 Köln 90
West Germany

ABSTRACT

Laser measurements and 3D-viscous calculations were performed to verify the design of a 30deg. backswept impeller with advanced blade geometry and high design rotor pressure ratio (π_{t12}=4.7:1). Both, measured and calculated results are in good agreement. They are pointing to a low velocity area inside the rotor that vanishes toward the exit resulting in comparatively smooth discharge velocity profiles. The rotor geometry used for the verification is released. The application of the 3D-viscous calculation code now embedded in an impeller design procedure and its support by a number of pre- and postprocessing programs is described.

NOMENCLATURE

c	= absolute velocity
c_m/u_2	= meridional velocity / tip speed
HU	= hub
$\dot{m}$	= mass flow rate
N_s	= specific speed (US units)
n/n_o	= shaft speed / design speed
PS	= pressure side
SH	= shroud
SS	= suction side
u	= circumferential velocity
x/s_m	= dimensionless shroud length
y/t	= dimensionless blade pitch
z/b	= dimensionless channel depth
η_{stt}	= total/total isentropic efficiency
π_t	= total pressure ratio

SUBSCRIPTS

0	= ambient condition
1	= impeller inlet
2	= impeller exit
3	= vaned diffuser inlet
4	= diffuser exit
red	= corrected

INTRODUCTION

Flow range and efficiency of centrifugal compressor stages are significantly influenced by the rotor- and diffuser flow characteristics. Both components are interacting on each other primarily in the impeller exit-/diffuser inlet area. Here, the impeller exit flow is very often disturbed by distorted static pressure fields and/or shocks generated by vaned diffusers that are usually applied for high pressure ratio stages (π_{t14}>4). On the other hand the diffuser inlet conditions are determined by the rotor discharge flow. Especially the fluctuations of the flow vector's magnitude and the unsteadiness in flow direction at the diffuser leading edge have been found to be due to the jet/wake pattern discharged by the rotor (Krain, 1981). Therefore designers of centrifugal rotors are generally aiming at smooth impeller discharge flow patterns which prerequisites theoretical models capable of correctly predicting the complex 3D-viscous flow field of centrifugal compressor impellers.

Some 3D-codes were already applied for modeling the flow fields of centrifugal impellers even at off-design conditions. Most calculations, however, were carried out for modest pressure ratios and ancient impeller designs (Dawes, 1988; Hah et al., 1988; Moore et al., 1988; Lapworth et al., 1988). This seems to be due to a lack of test cases and useful experimental data about today's high pressure ratio impellers.

This paper describes experiences made with a 3D-viscous code (Dawes, 1988) which is now a mo-

Presented at the Gas Turbine and Aeroengine Congress and Exposition—June 4-8, 1989—Toronto, Ontario, Canada

dule of an impeller design method (Krain, 1984) that has been coupled with pre- and postprocessing programs of a numerical flow simulation program system (FLOWSIM) developed at DFVLR (Hoffmann, 1986, 1987). These programs were used to verify a modern impeller design by detailed comparisons between laser measurement results and calculated data.

IMPELLER GEOMETRY AND PERFORMANCE CHARACTERISTICS

The rotor used for the verification was a low specific speed N_s=80 (US), 30 deg. backswept impeller running with 470 m/s tip speed (Krain, 1988).

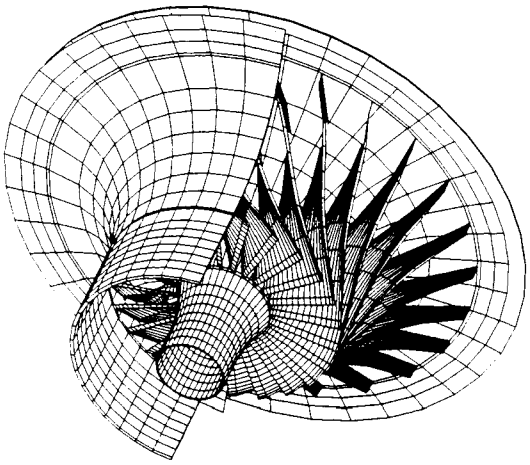

Fig. 1 Impeller design grid

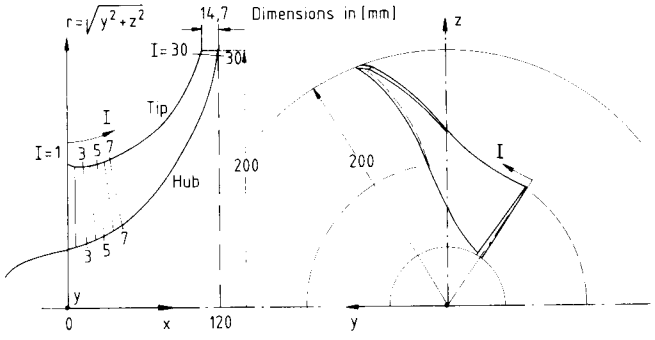

Fig. 2 Impeller Geometry

Fig.1 shows a 3D-plot of the impeller covered with the blade-design grids. The impeller has 24 full blades and was designed for a mass flow rate of 4.0 kg/s and a shaft speed of 22 363 rpm. The corresponding total rotor pressure ratio was 4.7:1. The blade geometry, given in cartesian coordinates, is submitted in Table I. Fig.2 illustrates the orientation of the cartesian coordinate system used. The blade surfaces are generated by straight lines which is a precondition for a flank-milling manufacturing process on a 5-axis NC-milling machine.

The measurement data were taken when the impeller was coupled with a vaneless diffuser of constant area. For performance measurements total temperatures and total pressures were measured at the compressor inlet and exit. Fig.3 shows the stage performance characteristics (Krain, 1988).

	PRESSURE SIDE						SUCTION SIDE					
	HUB			TIP			HUB			TIP		
I	X (MM)	Y (MM)	Z (MM)	X (MM)	Y (MM)	Z (MM)	X (MM)	Y (MM)	Z (MM)	X (MM)	Y (MM)	Z (MM)
1	0.00	-27.76	35.41	0.00	-65.64	91.67	0.00	-23.88	38.14	0.00	-63.92	92.88
2	6.40	-26.03	39.76	5.36	-57.95	96.86	6.40	-21.66	42.31	5.36	-55.46	98.31
3	12.70	-24.40	43.97	10.53	-51.16	101.01	12.70	-19.63	46.30	10.53	-48.11	102.50
4	18.90	-22.82	48.15	15.52	-45.07	104.49	18.90	-17.74	50.24	15.52	-41.65	105.90
5	24.98	-21.23	52.36	20.35	-39.55	107.51	24.98	-15.94	54.21	20.35	-35.89	108.78
6	30.93	-19.62	56.64	25.04	-34.50	110.22	30.93	-14.19	58.24	25.04	-30.70	111.34
7	36.76	-17.97	61.01	29.61	-29.82	112.73	36.76	-12.44	62.38	29.61	-25.97	113.68
8	42.44	-16.25	65.49	34.05	-25.46	115.10	42.44	-10.67	66.63	34.05	-21.60	115.89
9	47.98	-14.45	70.08	38.39	-21.36	117.40	47.98	-8.86	71.01	38.39	-17.53	118.03
10	53.37	-12.57	74.79	42.64	-17.48	119.66	53.37	-6.97	75.52	42.64	-13.70	120.16
11	58.59	-10.59	79.62	46.80	-13.77	121.93	58.59	-4.99	80.16	46.80	-10.04	122.29
12	63.64	-8.49	84.56	50.88	-10.21	124.22	63.64	-2.91	84.94	50.88	-6.53	124.47
13	68.52	-6.28	89.62	54.89	-6.75	126.57	68.52	-0.72	89.84	54.89	-3.12	126.71
14	73.22	-3.93	94.79	58.82	-3.39	128.99	73.22	1.60	94.86	58.82	0.21	129.04
15	77.72	-1.44	100.06	62.68	-0.07	131.51	77.72	4.05	99.99	62.68	3.50	131.46
16	82.03	1.20	105.43	66.47	3.20	134.13	82.03	6.63	105.22	66.47	6.75	134.00
17	86.14	4.00	110.88	70.18	6.48	136.88	86.14	9.35	110.56	70.18	10.01	136.66
18	90.04	6.97	116.41	73.80	9.77	139.76	90.04	12.21	115.98	73.80	13.28	139.47
19	93.73	10.12	122.00	77.34	13.11	142.80	93.73	15.23	121.47	77.34	16.59	142.44
20	97.20	13.46	127.66	80.79	16.52	146.00	97.20	18.40	127.04	80.79	19.95	145.57
21	100.45	16.99	133.35	84.12	20.04	149.38	100.45	21.73	132.66	84.12	23.38	148.89
22	103.48	20.73	139.07	87.32	23.68	152.93	103.48	25.24	138.32	87.32	26.92	152.40
23	106.27	24.68	144.81	90.37	27.49	156.67	106.27	28.93	144.02	90.37	30.57	156.10
24	108.83	28.85	150.54	93.25	31.48	160.60	108.83	32.82	149.73	93.25	34.37	160.01
25	111.15	33.25	156.26	95.92	35.68	164.72	111.15	36.92	155.43	95.92	38.34	164.12
26	113.23	37.88	161.94	98.36	40.13	169.01	113.23	41.26	161.12	98.36	42.53	168.42
27	115.07	42.75	167.58	100.52	44.83	173.46	115.07	45.84	166.76	100.52	46.95	172.90
28	116.66	47.87	173.14	102.37	49.80	178.06	116.66	50.69	172.34	102.37	51.65	177.53
29	118.00	53.26	178.62	103.86	55.06	182.78	118.00	55.82	177.83	103.86	56.66	182.29
30	119.09	58.91	183.98	104.95	60.62	187.60	119.09	61.26	183.21	104.95	62.02	187.15

Table I: Blade Coordinates

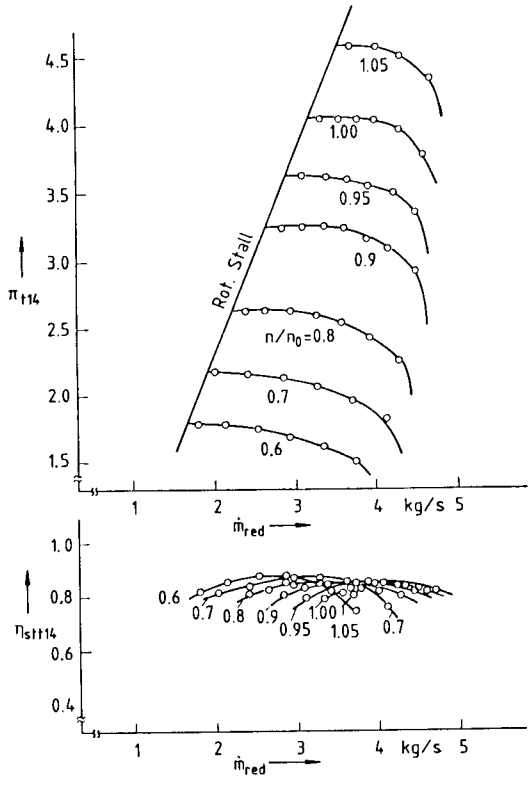

Fig. 3 Performance map of the centrifugal compressor stage composed of the backswept impeller and a vaneless diffuser

NUMERICAL PROCEDURE

The numerical simulation of the 3D-viscous impeller flow is carried out by a number of coupled programs for impeller design, 3-D Navier Stokes solution, grid generation and flow visualization (Fig.4).

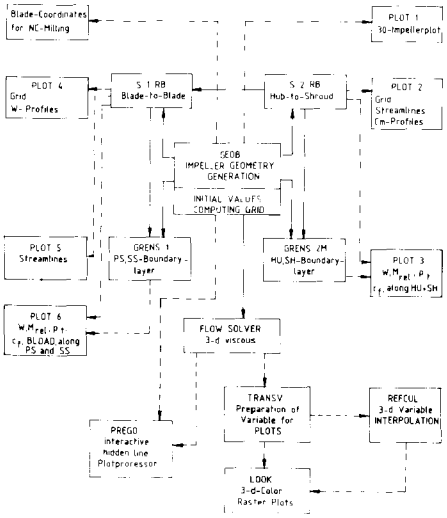

Fig. 4 Program package for impeller design, flow field analysis and 3D-data visualisation

PREPROCESSING

The upper part of Fig.4 shows a block diagram of the DFVLR-impeller design procedure (Krain, 1984). The initial impeller optimization is carried out with a fast quasi-three dimensional calculation method based on Wu's streamsheet approach (Wu, 1952) that is coupled with a boundary layer calculation method. Finally an additional flow field analysis is carried out with the 3D-viscous code that gives insight into those flow phenomena that are not taken into account by the Q3D-approach. Due to the assumptions implied, Q3D-calculation methods are generally not capable to predict secondary flow and vortex developments because it is almost impossible to find suitable stream surfaces for these flow phenomena. This gap is filled by the 3D-code that can give more insight into the real flow physics especially if the postprocessing enables the user to get 3D-images of the calculated results.

3D-VISCOUS FLOW SOLVER

The simulation of the flow inside the high pressure ratio centrifugal compressor rotor demands for viscous field solutions able to find implicitly the edge of separation and handle transonic regions. Dominant Coriolis-forces in the radially directed rear part of the impeller cause strong vortex amplification and wake formation, which cannot be handled easily, if ever, by coupled inviscid-viscous solutions. The computer code of Dawes (1988) has been used to solve the time-dependent Reynolds-averaged Navier-Stokes-equations for the steady state flow at design point. The original code has been modified for use on IBM 3090 and Cray-XMP vector-computers. With regard to viscous length scales, a relatively coarse grid of 16x16x94 blade-to-blade, span- and streamwise finite volumes has been used, Fig.5. Tip clearance effects were modeled by using only one grid line in the gap.

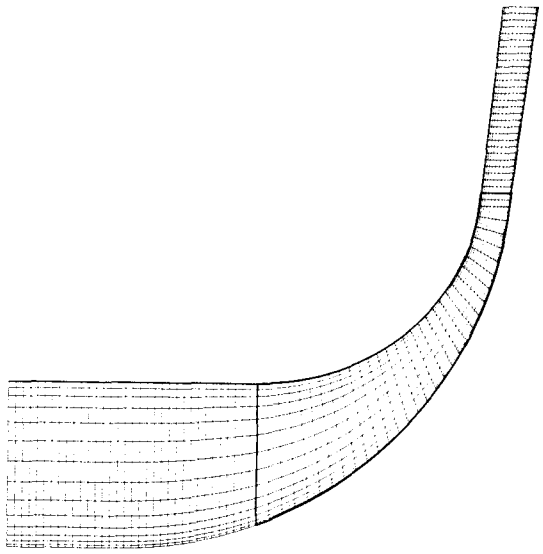

Fig. 5 3D-Computing grid

Nevertheless, computing times are still high, even for autovectorized runs. Thus, a new, highly vectorized code has been developed for use on a Cray XMP-216 with CPU times reduced by a factor of three compared to the original auto vectorized program. The rate of data processing now reaches 2.9×10^{-5} seconds per number of volumes and time steps. A further significant reduction is expected introducing multi-tasking and better suited volume numbers that avoid bank conflicts and guarantee optimum vector pipe loading. Besides this, the FAS-multigrid scheme will increase convergence when applied to more than the two grids currently in use.

POSTPROCESSING

Postprocessing is an essential part of the numerical procedure and plays an increasing role for the interpretation of solution data. Based on converged primary variable distributions including pressure, density, axial-, radial-, and tangential velocity, the postprocessing programs shown in the lower part of Fig.4 prepare the dependent secondary variables. The programs refine distributions up to 5×10^{5} finite volumes by 3-dimensional interpolation if recommended, calculate interactively hidden-line views of geometries and generate 3D arrows- or isocolour plots based on grid surfaces. Due to the large amount of postprocessing data, machine restrictions have forced the development of modular programs which may be started dynamically in a user-defined sequence.

With this, a flexible analysis of the computed flow field and implemented measurement data is available.

MEASUREMENT TECHNIQUE

The optical measurements carried out in the rotor area were performed with the Laser-Two-Focus (L2F) velocimeter developed at DFVLR (Schodl, 1980). This measurement system gives

information about the magnitude and direction of the mean absolute flow vector and its turbulent components. The components of the corresponding relative velocity vector are easily calculated with the help of the known circumferential velocity. Generally, the error in mean velocity measurements is below ±1 percent and the uncertainty in flow angle measurements is less than ±1deg.. The optical measurements inside the rotating system display the flow field development from the rotor inlet to the rotor exit thus giving information about the real flow process in the rotor. These data can be used to support advanced flow field theories.

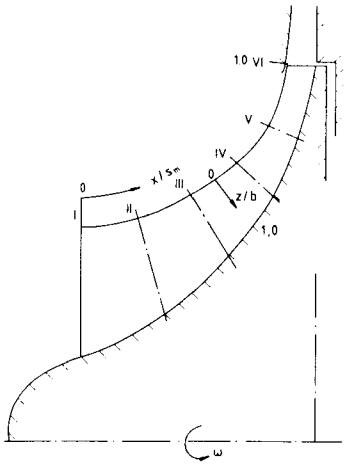

Fig. 6 Arrangement of L2F-measurement planes

Fig.6 shows the arrangement of the L2F measurement positions in the meridional plane of the backswept rotor that were used for the experimental analysis. All measurement planes are perpendicular to the shroud contour and they are located at 0, 20, 40, 60, 80 and 100.4 percent meridional shroud length. At each plane measurements were taken at 5 channel depths (z/b=0.1, 0.3, 0.5, 0.7, 0.9) and at about 13 to 14 circumferential positions. Thus the whole measured flow field is composed of about 400 measurement points.

LASER MEASURED DATA IN COMPARISON WITH NUMERICAL RESULTS

The following figures are illustrating the results of a comparison between measured and calculated data carried out for the rotor design point. At first, Fig.7 gives an impression about the overall flow development ahead of, inside, and aft of the rotor.

The relative Mach number distributions on cross-flow surfaces are shown by differently shaded areas. The corresponding Mach number values can be taken from the legend. Highest relative Mach numbers are present in the shroud leading edge area which is primarily due to the large circumferential relative velocity component present in this region.

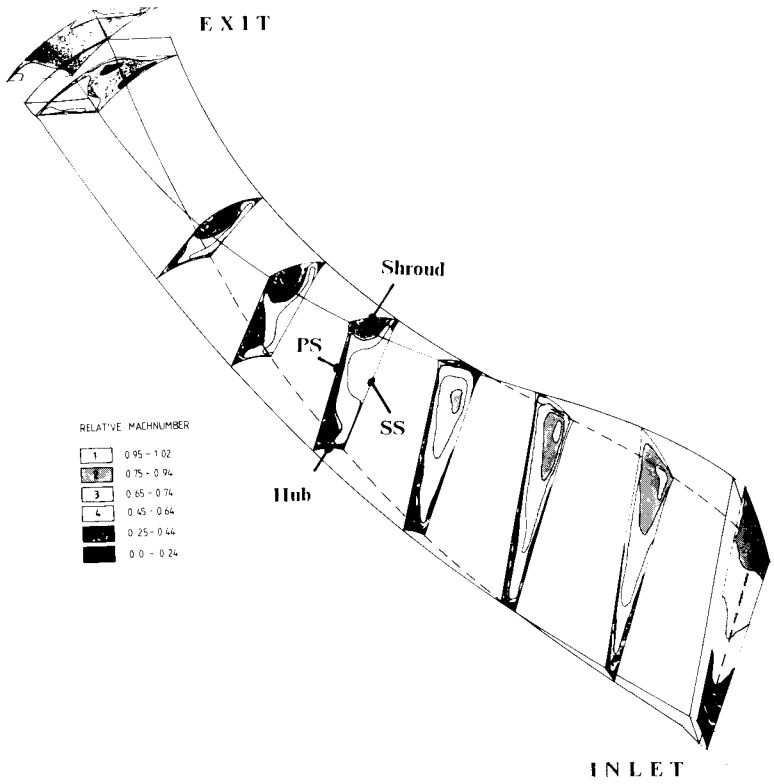

Fig. 7 Calculated relative Mach number distributions on cross-flow surfaces in the flow field
(n/n_o = 1, $\dot{m}$ = 4.0 kg/s)

Toward the hub the relative Mach number is dropping in the inlet area which is in agreement with the decreasing circumferential velocity and the assumption of an inlet flow without preswirl that corresponds with the real flow conditions. Inside the rotor the shroud Mach number is strongly decreasing from the leading edge up to 60 percent meridional flow path length. This tendency is reversed toward the impeller exit. The flow has totally mixed out at the exit of the calculation domain. Test calculations with prolonged grids showed similar distributions, indicating that the calculation area aft of the impeller has been chosen large enough.

Fig.8 shows perspective views of calculated hub-to-tip Mach number distributions close to the blade surfaces and at mid-pitch. The results clearly reveal an accumulation of low velocity fluid in the shroud area of the rotor. This region extends from about 20 to 70 percent flow path length. Toward the exit the 3D-viscous code predicts an acceleration of the relative flow resulting in a reduction of the low velocity area. Primarily at the mid-pitch surface (Fig.8b) this tendency is clearly seen. Figs.7 and 8 are pointing to an accumulation of low velocity fluid in the shroud area of the rotor what is in full agreement with the laser measurement results. Especially the velocity distribution from the impeller inlet to the exit is modeled quite good what

can be deduced from Fig.9 showing the measured and calculated meridional velocity profiles at the six measurement planes of Fig.6.

In Fig.9 the measured meridional velocities referred to the rotor tip speed (c_m/u_2) are indicated by circles and plotted versus flow area. Very regular velocity patterns and low blade loadings are present at planes I and II, whereas irregular velocity profiles have been measured in the shroud regions of planes III to VI. The velocity patterns of planes III to VI are indicating low velocity regions most pronounced at 60 percent meridional flow path length and disturbed velocity profiles that are smoothing out toward the impeller exit.

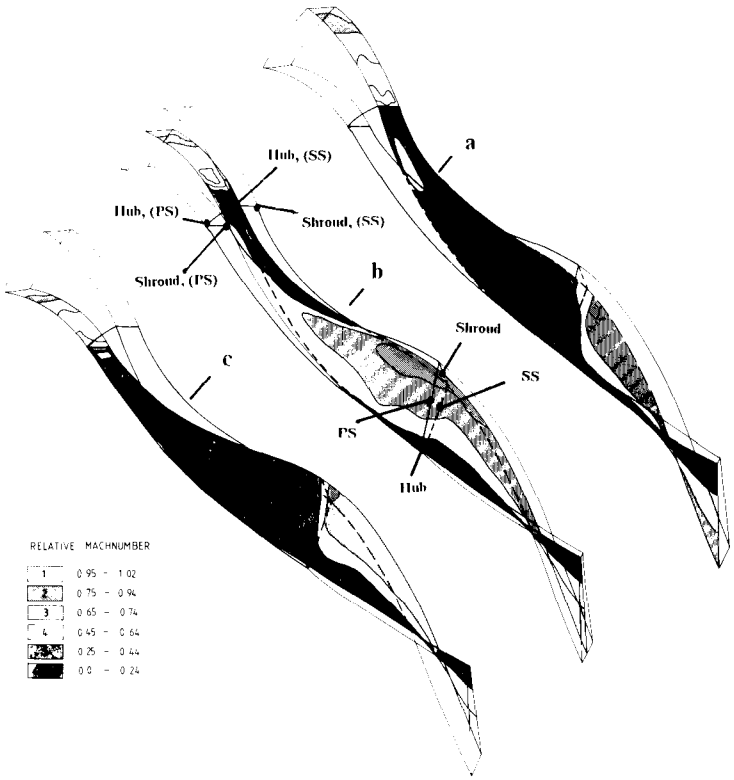

Fig. 8 Calculated relative Mach number distribution on hub-to-tip surfaces, located close to the suction side (a), at mid-pitch (b) and close to the pressure side (c). (n/n_o = 1, $\dot{m}$ = 4.0 kg/s)

The disturbances have been appointed to the vortex development deduced from the measured relative flow angle distributions (Krain, 1988). The comparison with Figs.7 and 8 shows that the 3D-viscous calculation method predicts the same tendency in the throughflow direction. The location of the low velocity area is predicted quite good.

Fig.9 additionally shows a quantitative comparison between measured and calculated data for all measurement planes. A good agreement between calculation and measurement is obtained at planes I and II. A good agreement is also obtained for plane III located at 40 percent flow path length. The measured

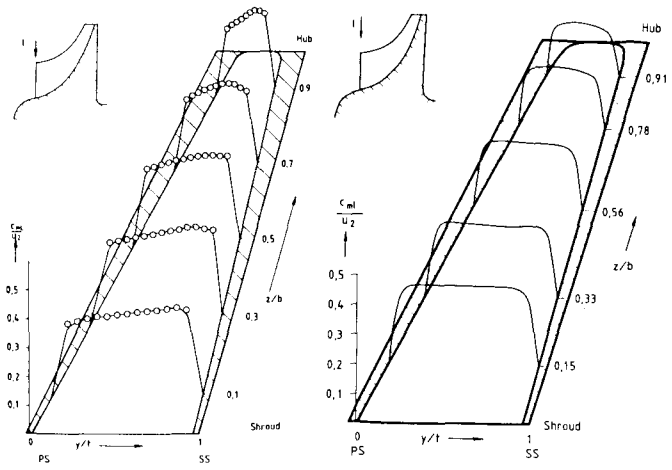

Measured Calculated
Fig. 9 Plane I

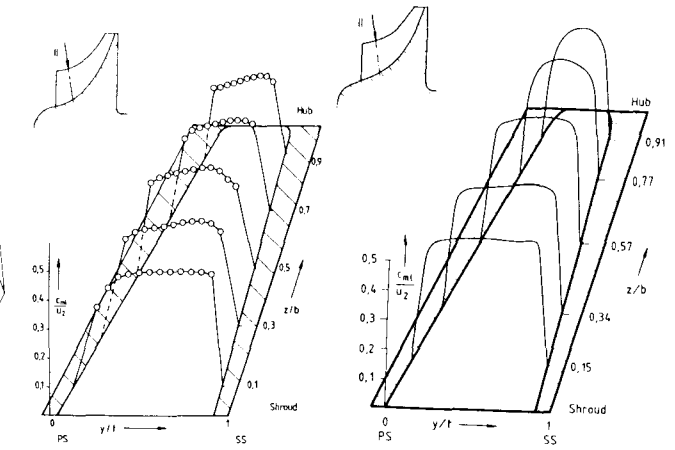

Measured Calculated
Fig. 9 Plane II

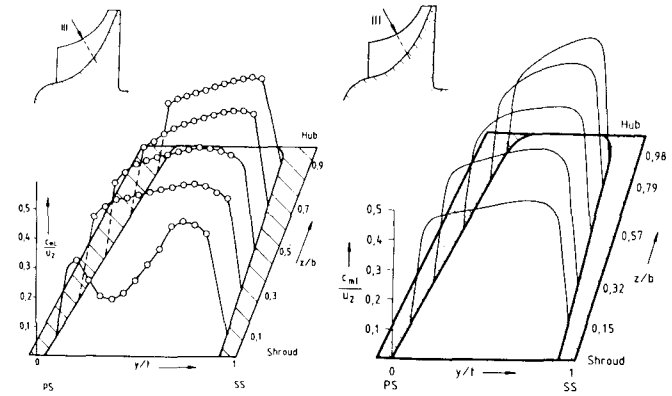

Measured Calculated
Fig. 9 Plane III

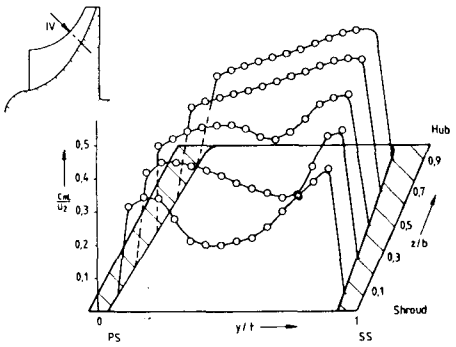

Measured

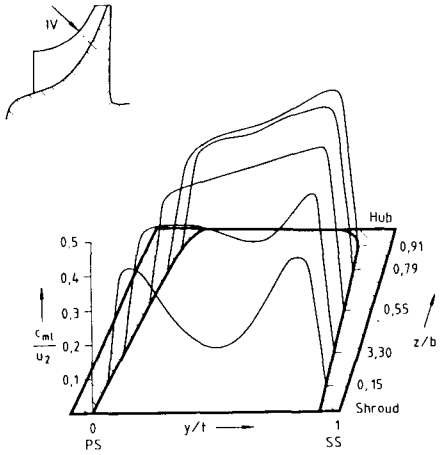

Calculated

Fig. 9 Plane IV

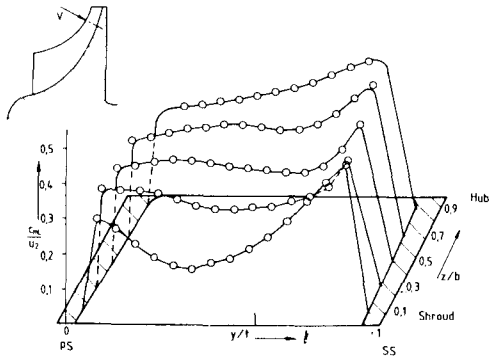

Measured

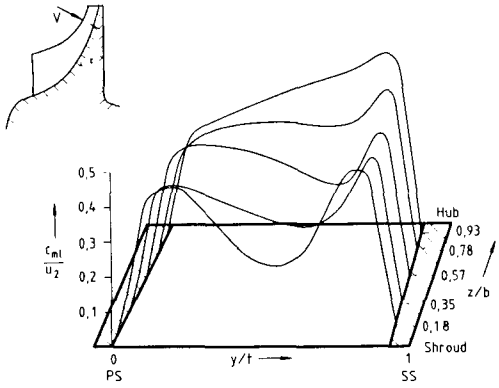

Calculated

Fig. 9 Plane V

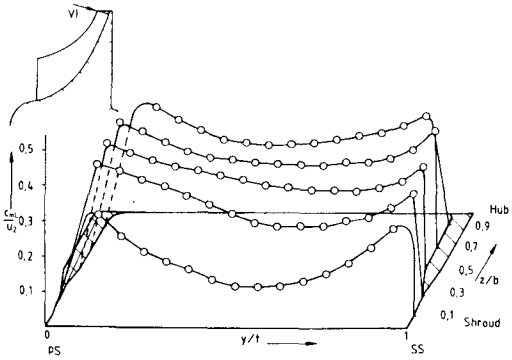

Measured

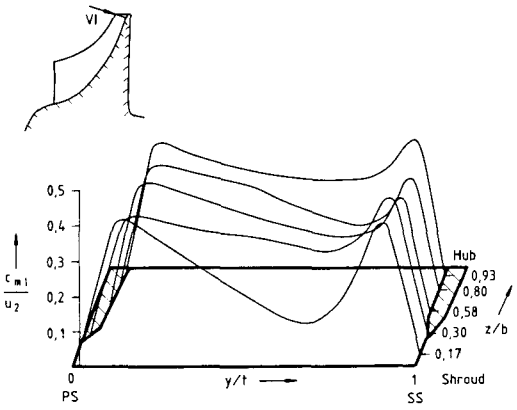

Calculated

Fig. 9 Plane VI

Fig. 9: Meridional velocity profiles measured and calculated at planes I-VI (n/n_o = 1, $\dot{m}$ = 4.0 kg/s)

disturbance in the shroud area (z/b=0.1) at this position has only a small extension in the z/b-direction. This disturbance is not seen in the plot of the calculated results since this plot shows the first velocity profile at 15 percent channel depth. At plane IV measured and calculated meridonal velocity profiles are indicating the low velocity areas at almost the same position. Minimum velocities are located close to the shroud and at the middle of the flow channel. Both the theoretical as well as the experimental results are indicating disturbed velocity profiles covering more than 30 percent of the channel depth. At plane V the extension of the disturbed velocity profile in the z-direction is again correctly predicted and the calculated meridional velocity distributions in the circumferential direction agree also fairly good with the measurements. In the shroud area calculated and measured profiles are

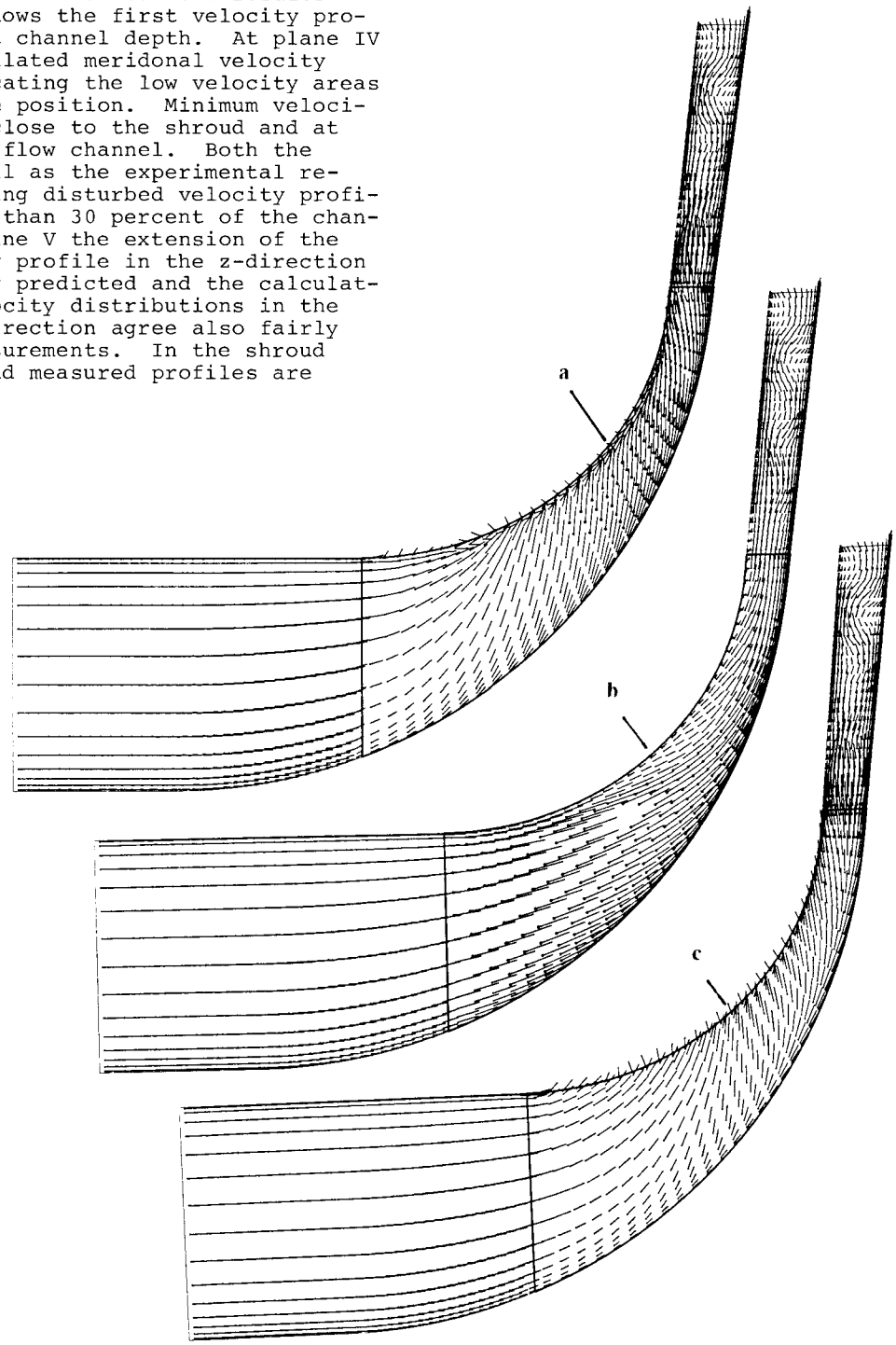

Fig. 10: Calculated meridonal velocity distributions close to the suction side (a), at mid-pitch (b) and close to the pressure side (c) (n/n_o = 1, $\dot{m}$ = 4.0 kg/s)

similar to those of planes III and IV with a minimum almost at mid-pitch and rising velocities toward the blade surfaces pointing to a vortex development (Krain, 1988).

At plane VI calculated and measured results are showing good agreement especially with respect to blade loading. Both the theoretical and experimental results are pointing to a very low blade loading accompanied by a smooth velocity distribution. Obviously a pronounced jet/wake-type flow found at the exits of several other centrifugal compressor impellers (Hah et al., 1988; Lapworth et al., 1988; Krain, 1981) is neither predicted nor measured. As indicated in Fig.9 the measurement positions z/b=0.1 and z/b=0.3 are already outside of the rotor. The velocity profiles plotted for those positions are no longer representing the impeller flow they are illustrating the flow character in the diffuser inlet area. Zero blade thicknesses at those positions result in a sudden drop of meridional velocity clearly seen in plane VI.

Finally, Fig.10 shows calculated velocity distributions in three meridional planes located close to the suction side, at mid-pitch and close to the pressure side of the blade. The surfaces located in the vicinity of the blades (Figs.10a, 10c) give information about the secondary flows present in the corresponding boundary layers. As expected, the flow vectors are primarily directed toward the shroud resulting in an accumulation of low throughflow velocities in the shroud area. At both surfaces this tendency is most pronounced from about 20 to 70 percent flow path length. In the inlet and exit areas of the rotor, however, the meridional velocities are almost parallel to the hub and shroud surfaces. At mid-channel (Fig.10b) the flow is well guided with almost no hub-to-shroud secondary flows. The meridional velocity plot at mid-pitch clearly shows an area of low velocity fluid in the shroud region which agrees with the measurement results of Fig.9. The accumulation of low velocity fluid in this region seems also to be due to the high relative velocity deceleration in that area what was deduced from calculations neglecting tip clearance effects. In fact, during the design process the highest deceleration was set to the inlet area because the boundary layer calculations performed show this to be the best way for obtaining a high overall deceleration without separation.

CONCLUSIONS

The verification of an impeller design performed by a detailed comparison between laser measurement data and theoretical results revealed that the 3D-viscous code used is capable of correctly predicting the location of the low velocity region in the through flow direction. The calculations confirmed the absence of a classical jet/ wake pattern at the exit of the backswept impeller. Noticeable differences between measurement and calculation occurred only in the vicinity of the shroud. The 3D-viscous code was found to give a good insight into the flow development of an impeller with complex blade geometry, primarily if a well developed post-processing program system is available. Since the code is now part of an impeller design package it will probably become a useful tool for future designs.

REFERENCES

Dawes, W.N., 1988, "Development of a 3D Navier Stokes Solver for Application to all Types of Turbomachinery". ASME-Paper 88-GT-70.

Hah, C.; Bryans, A.G.; Moussa, Z.; Tomsho, M.E., 1988, " Application of Viscous Flow Computations for the Aerodynamic Performance of a Back-Swept Impeller at Various Operating Conditions". ASME-Paper 88-GT-39.

Hoffmann, W., 1986, "Grid Generation Programsystem HGRID". DFVLR, Institut für Antriebstechnik, IB-325-11-86.

Hoffmann, W., 1987, "Graphical Presentation of Computational Grids, Program System PREGEO". DFVLR, Institut für Antriebstechnik, IB-325-08-87.

Krain, H., 1981, "A Study on Centrifugal Impeller and Diffuser Flow". ASME Journal of Engineering for Power, Vol.103, No.4, Oct. 1981, pp.688-697.

Krain, H., 1984, "A CAD-Method for Centrifugal Compressor Impellers". ASME Journal of Engineering for Gas Turbines and Power, Vol.106, April 1984, pp.482-488.

Krain, H., 1988, "Swirling Impeller Flow". ASME Journal of Turbomachinery, Vol.110, Jan. 1988, pp.122-128.

Lapworth, B.L., Elder, R.L., 1988, "Computation of the Jet-Wake Flow Structure in a Low Speed Centrifugal Impeller". ASME-Paper 88-GT-217.

Moore, J.G.; Moore, J., 1988, "Secondary Flow, Separation and Losses in the NACA 48-Inch Centrifugal Impeller at Design and Off-Design Conditions". ASME-Paper 88-GT-101.

Schodl, R., 1980, "A Laser-Two-Focus (L2F) Velocimeter for Automatic Flow Vector Measurements in the Rotating Components of Turbomachines". ASME-Paper, No.1980, In Measurement Methods in Rotating Components of Turbomachinery, pp.139-147.

Wu, C.H., 1952, "A General Theory of Three-Dimensional Flow in Subsonic and Supersonic Turbomachines of Axial, Radial and Mixed-Flow Types". NACA TN-2604, 1952, p.92.